JOURNAL OF MATERIALS SCIENCE 17 (1982) 2525–2532

TEM investigation of crystallization phenomena in the metallic glass Vitrovac® 0040 ($Fe_{40}Ni_{40}B_{20}$)

K. MÜLLER, M. VON HEIMENDAHL
Institut für Werkstoffwissenschaften I der Universität Erlangen-Nürnberg, Martensstrasse 5, D-8520 Erlangen, West Germany

The crystallization behaviour of the amorphous alloy $Fe_{40}Ni_{40}B_{20}$ was investigated by transmission electron microscopy (TEM) and light microscopy. The three different types of crystals, which occur simultaneously in the temperature range between 355 and 385° C, were formed by *time-dependent* or *athermal* nucleation, respectively. The number of such athermally formed nuclei increases with decreasing quench speed, whereas the time-dependent nucleation is not influenced. The linear growth of all three crystal types is likewise independent of the quenching rate. Although the activation energies for growth, E_g, are the same for all three types, there are great differences in growth rates, and therefore the thermal stability against crystallization is controlled by the fastest-growing type of crystal. Furthermore, a mechanical treatment or plastic deformation may produce surface crystallization.

1. Introduction

The amorphous alloy $Fe_{40}Ni_{40}B_{20}$ has been investigated in many respects, due to its technical relevance and interesting magnetic properties. However, very little has been reported on the important question of thermal stability and crystallization behaviour. The few published papers [1–3] do not give a complete and clear picture of it. This study was therefore undertaken to assess the crystallization behaviour in the light of our former systematic studies on other FeNi-base metallic glasses [4–8]. This concerns the separate measurements of activation energies for crystallization, E_c, nucleation, E_n, and growth of crystals, E_g, by means of quantitative microscopy, in conjunction with integrating measurements such as differential thermal analysis (DTA) and differential scanning calorimetry (DSC).

2. Experimental procedure

The amorphous ribbons were kindly supplied by Vacuumschmelze GmbH, Hanau. The different charges used are listed in Table I. Charge number 3 had a faster quench speed than the others, corresponding to the smaller thickness (factor 0.5). A wet chemical analysis proved the nominal alloy composition to be correct within ± 0.5% (all values in at.%). Heat treatments in a salt bath were performed as described earlier [9], the achieved temperature stability being better than ± 0.5 K oscillations (absolute value of temperature read out ± 2 K). TEM sample preparation [10] has been described before [9]; for details of the present application see [11]. A mixture of 80% ethanol and 20% perchloric acid was used for electropolishing at −33° C, 10 V in a Tenupol apparatus (flow rate = 10). However, no more than 50% of useful disk specimens were attained.

To obtain the number of nuclei (crystals) per μm^3, N_v, the number per μm^2 area, N_a, taken from the picture, must be divided by $\bar{D}$, the mean

TABLE I Vitrovac charges used in this work

Charge No.	Number of producer	Width (mm)	Thickness (μm)
1	C 393	3	45
2	– 717	3	45
3	C 1586	1	24
4	E 170	20	42

0022–2461/82/092525–08$03.46/0

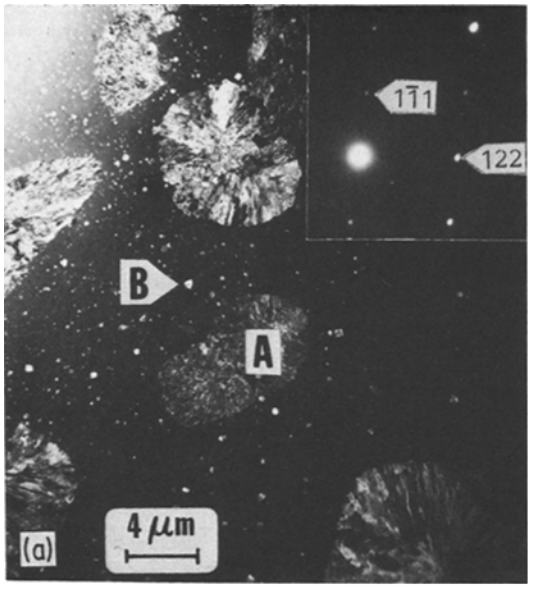

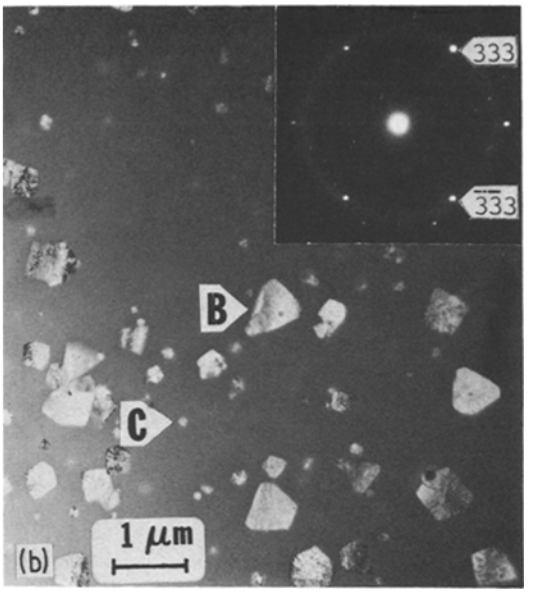

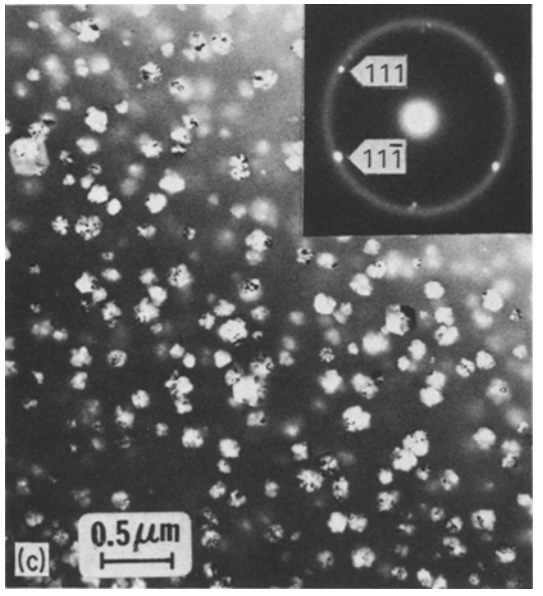

Figure 1 Different types of crystals in $Fe_{40}Ni_{40}B_{20}$ (with diffraction patterns): (a) type A (large): γ-FeNi + $(FeNi)_3B$; (b) type B (medium): γ-FeNi + $(FeNi)_{23}B_6$; (c) type C (small): γ-FeNi.

particle diameter [12]: $N_v = N_a/\bar{D}$ in the case of optical microscopy. For TEM the corresponding formula is $N_v = N_a/(\bar{D} + t)$, where t is the TEM specimen thickness. Because of the difficulty in measuring it in any individual case, it was taken as 100 nm i.e., the average value determined by thickness measurements after [13] or [14].

For faster evaluation of electron diffraction spot patterns, the basic seven rules described in Chapter 3.6 of [10] were worked out by a tailor-made semi-automatic computer program, run on a diskette in the EDAX 9100/60 (DEC RT-11 computer); see [11].

3. Results and discussion

3.1. Crystal types and structures

At first, the amorphous as-quenched state was checked. In the TEM the appearance was completely homogeneous, no quenched-in crystals, other impurities or heterogenities could be detected. Also electron diffraction patterns showed only diffuse rings.

Surprisingly, the alloy crystallized simultaneously in three different types of crystals. This is true for all four temperatures used: 355, 365, 375 and 385° C. Such behaviour was not observed in the earlier investigated Fe–Ni based amorphous alloys [4, 6, 9] and should not be confused with the sequences of metastable phases called MSI and MSII, e.g., in the Metglas® 2826A, [4, 9]. Fig. 1a to c present the three very different crystal sorts – notice the steps in magnification. In Fig. 1a the much smaller crystals of type B are only to be seen in the background in contrast to the large crystals of type A. The same is true for Fig. 1b, where the small crystals (type C) are in contrast to the larger, sharply defined type B crystals. Table II summarizes the characteristics of the crystals, obtained by TEM and the diffraction patterns (shown as inserts in the figures).

In Fig. 1b the exact orientation relationship between the two eutectic phases leads to a super-

TABLE II The three types of crystals in $Fe_{40}Ni_{40}B_{20}$ (lattice parameter values are mean values for the Fe- and Ni-compounds, respectively)

Type	Structure and morphology
A (large)	Eutectic: γ-FeNi + $(FeNi)_3B$ orthorhombic with $a = 0.442$, $b = 0.530$ and $c = 0.663$ nm. Irregular shape of contours, no regular crystal shape. Eutectic phases clearly recognizable.
B (medium)	Eutectic: γ-FeNi + $(FeNi)_{23}B_6$ f c c with $a = 1.07$ nm. Characteristic shape of clear, straight lined crystal contours. Eutectic structure again clearly visible.
C (small)	Single phase γ-FeNi, f c c with $a = 0.358$ nm. Roughly spherical, partly dendritic crystal shape.

position of every third $(FeNi)_{23}B_6$ reflection with a reflection of γ-FeNi, whose lattice parameter is three times smaller than $(FeNi)_{23}B_6$.

An X-ray investigation of the fully crystallized ribbon resulted only in the Debye–Scherrer lines of the $(FeNi)_3B$ phase from type A crystals. Stubicar *et al.* [2] also found only this phase in the same alloy. The probable reason is that this phase forms the largest crystals, strongly dominant in terms of volume. Only the much more sensitive TEM and SAD techniques revealed the existence of the other two phases in the present work. Cziraki [3] also found $(FeNi)_3B$ exclusively, although TEM was used. The phase $(FeNi)_{23}B_6$, being metastable, was reported earlier [15] as a possible phase occurring in the FeNiB-system and also by Herold and Köster [16], however in the FeB two-component system as $Fe_{23}B_6$.

Summarizing, it can be said that the typical appearance of the three distinctly different types of crystals in $Fe_{40}Ni_{40}B_{20}$ seen in TEM in this work were not reported earlier. The reason for the simultaneous growth of these three types was somewhat puzzling in the beginning, but will be discussed and explained later.

It also seems interesting that, in contrast to $Fe_{40}Ni_{40}B_{20}$, the alloys $Fe_{80}B_{20}$, $Fe_{50}Ni_{30}B_{20}$ [17] and $Fe_{40}Ni_{40}P_{14}B_6$ [18] all from a *tetragonal* boride $(FeNi)_3B$ with $a = b = 0.863, c = 0.429$ nm, and not the orthorhombic structure of type A. The question is why the differences in metal or metalloid content cause this change in crystal structure. A possible explanation might be the interaction between Fe and P on one hand and between Ni and B on the other hand, as suggested by Wong *et al.* [19]. One also has to keep in mind the phase change b c c to f c c at about 40% Ni in the Fe–Ni system.

3.2. Nucleation behaviour of the three crystal types

To judge the thermal stability, nucleation and growth must both be assessed in detail. Using the techniques of quantitative metallography as described in Section 2, the kinetics shown in Fig. 2a to c for types A to C were obtained. For type C crystals, after a certain incubation time, a linear increase in crystal densities indicates a

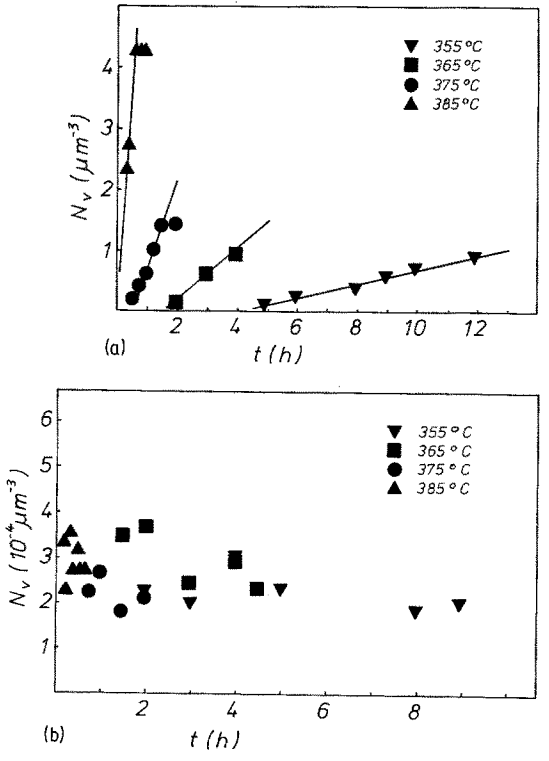

Figure 2 Number of crystals N_v of the three types of crystals after isothermal annealings: (a) type C (from TEM); (b) Type A (from LM); (c) type B (from TEM).

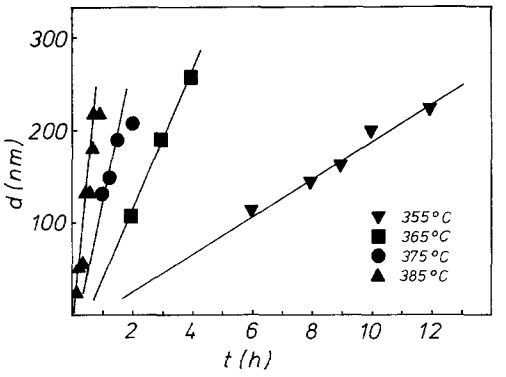

Figure 3 Growth of crystal of type C against time in isothermal annealing.

constant nucleation rate $\dot{N}_v$. This is true for all four temperatures investigated. This continuous nucleation process results in N_v depending on time due to the thermally activated nucleation process. In contrast, for types A and B crystals Figs 2b and c show quite a different behaviour: N_v is roughly time-independent, within experimental scatter it depends neither on time nor temperature. (The scatter is due to the limited number of crystals observable and counted.)

These cases of a constant nuclei number can, however, have two different reasons:

(1) heterogeneous nucleation on impurities;

(2) "athermal" nucleation [20], i.e., nuclei belonging to the system in the thermodynamic sence, which are formed during cooling of the melt.

A choice between these two possibilities is made in Section 3.4.

3.3. Growth characteristics of the three crystal types

The sizes of the largest crystals are measured by light optical microscopy (LM) for type A and by TEM for types B and C. Fig. 3 shows that the γ-FeNi primary crystals of type C grow linearly with time for all four temperatures. This is contrary to [1] where a $t^{1/2}$ proportionality, i.e. parabolic growth, was observed for the same alloy. In our case, growth seems to be governed by an interface-controlled reaction. Also, our type C crystals are larger and less numerous than in [1].

For a eutectic reaction, which is clearly interface-controlled, a linear-time growth is expected. This was also observed for types A and B, resulting in plots very similar to Fig. 3. Growth rates could be measured to be as follows: for type B 74, 190, 420 and 910 nm h^{-1} for 355, 365, 375 and 385° C respectively; and for type A 2.0, 4.6, 10 and 28 μm h^{-1} for the same temperatures, respectively. The values for type A are in good agreement with [1]; type B was not reported there.

It is surprising, and not yet understood, why the two eutectic types, which grow simultaneously, have such a difference in growth rate. A possible reason could be a different accommodation factor for the elementary step per atom settling in the crystal–glass interface. Anyway, in cases like this a determination of diffusion coefficients D via lamellar spacings λ and growth rate $\dot{d}$, as treated in [20], is an extremely problematic matter.

3.4. Influence of quenching speed

The faster quench speed of charge 3 (all others being nominally equal and lower) allows some conclusion concerning the nucleation processes of types A and B. Table III summarizes N_v and d_{max} for all four charges in a fixed (t, T)-situation.

It is very interesting to note that:

(1) the three different types A, B and C occur in all charges;

(2) growth is the same, independent of production conditions;

(3) nucleation of type C is also charge-independent;

(4) nuclei density of the eutectic crystals of types A and B is only less than 1/2 to 1/3 in the faster quenched charge 3.

This latter fact now proves inequivocally that nucleation of types A and B is not heterogeneous, but athermal, because N_v varies with quench

TABLE III d_{max} and N_v after 30 min at 385° C for four charges

Charge no.	$(FeNi)_3B$		$(FeNi)_{23}B_6$		γ-FeNi	
	d (μm)	$N_v(10^{-4}$ μm$^{-3})$	d (nm)	$N_v(10^{-2}$ μm$^{-3})$	d (nm)	N_v(μm^{-3})
1	11	2.2	370	2.8	130	4.2
2	11	3.3	370	2.9	130	4.4
3	11	0.9	370	1.2	130	4.8
4	11	3.6	370	3.2	130	4.9

speed. A heterogeneous nucleation at the site of impurities depends only on their number, whereas the slower the quench speed the more nuclei have time to develop during quenching to room temperature. At the crystallization temperature, these nuclei are then larger than the critical nucleus size.

It should be mentioned that the three type of crystals also occurred in a ribbon spun in our laboratories*, for the melt using the same alloy material as above, i.e., made by Vacuumschmelze GmbH.

3.5. Activation energies

It has recently been pointed out by Leake and Greer [21], that there are certain pitfalls with determination of the activation energy for crystallization, E_c, via DTA or DSC. These quite often overlooked difficulties concerning the heat transfer between furnace and sample, sample mass, and so on. Therefore, in the present work we determined the activation energies for nucleation, E_n, and for crystal growth, E_g, by TEM, as done already for the Metglasses® 2826A [4] and 2826 [6]. From Fig. 2a the slopes of the four lines yield $\dot{N}_v(T)$. Using the Arrhenius plot for $\ln \dot{N}_v$ against $(1/T)$, the value for E_n (type C) = 440 ± 30 kJ mol^{-1} follows. (For the two athermally formed types A and B, of course, no E_n can be derived.) Concerning growth, E_g is obtained from $\dot{d} = d_0 \times \exp(-E_g/RT)$ for constant $\dot{d}$ at each temperature, i.e., linear-time growth, which is the case for all three species. Values of $\dot{d}(T)$ were taken from Fig. 3 and the corresponding plots for types A and B, not reproduced here. The Arrhenius plots, $\ln \dot{d}$ against $(1/T)$, again yielded good straight lines with the result that the activation energies for all three types were the same: $E_g = 280 \pm 30$ kJ mol^{-1}. The absolute values of $\dot{d}$ are, however, as mentioned above, very different (70:3:1 for types A, B and C. respectively), which means that the Arrhenius lines for the three types are parallel but shifted with respect to each other (Fig. 4).

The value $E_g = 280$ kJ mol^{-1} is in good agreement with that of Herold and Köster [1]; they found 270 kJ mol^{-1} for the crystals corresponding to our type A. The fact that all three types have the same E_g, explains the simultaneous occurrence in the whole observed temperature range: different

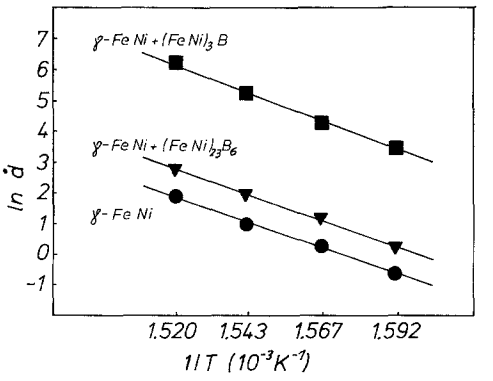

Figure 4 Arrhenius plot for obtaining the activation energies for growth, E_g.

E_g would have the consequence that very soon one species would dominate.

Our recently developed formula [5] for E_c as a function of E_n and E_g cannot actually be applied in cases like this, where more than one crystal species grows simultaneously. By the same token, the determination of E_c via DTA is also somewhat of a problem. Therefore, we also use E_n and E_g for the following considerations on thermal stability.

3.6. Thermal stability

The time at which a metallic glass starts to crystallize, and how fast this process goes on, is of fundamental importance for technical applications of these materials. Both processes, nucleation and growth, need careful consideration in this context. Generally, the ternary FeNiB alloys are more stable against nucleation than the binary alloy FeB [22]. (Also, according to Luborsky [23], the higher the number of elements in the alloy, the higher E_c.)

The question arises whether thermal stability is influenced differently by the three types or not. To judge this, we consider the relationships of N_v and d. For types A and B, N_v is roughly constant; for type C (T, t)-dependent. However, for an order-of-magnitude estimate we see from Figs 2a to c that the N_v are related as given in Table IV.

The d- and d^3-relations are independent of T, because E_g is the same for all three types. It follows from Table IV that although N_v is very small for type A, this is by far outweighed by the faster growth due to the fact that volume is

*The authors are grateful to Professor Dr A. Hubert and Mr Grimm, Institut für Werkstoffwissenschaften VI, Universität Erlangen-Nürnberg, for this melt spinning.

TABLE IV Orders of magnitude for crystal numbers and volumes

	Type A	Type B	Type C
N_v	1	100	10 000
d	70	3	1
d^3	350 000	30	1

proportional to the third power of linear dimension. In other works, the few but very large type A crystals dominate in the volume. (This was the reason that only this type was detected by X-rays; see Section 3.1.) However, type C is strongly (T, t)-dependent. The lower T, the stronger is the influence of the athermal types A and B. In this context see also the schematic *TTT*-diagram Fig. 10.10 in [20]. On the other hand, at high T, type C crystals will play a greater role due to their greater $N_v(T, t)$ at high temperatures. For technical applications the start of nucleation is important i.e., the lower temperatures rather than high ones. Therefore, only the athermally formed nuclei are critical and responsible for thermal instability in this alloy. They should be avoided as much as possible by faster quenching speeds or other means.

3.7. Surface crystallization

So far, N_v dealt only with homogeneous, equally distributed nuclei, regardless of whether time-dependent or athermal. It is well known, however, that potential surface crystallization (SC) [24–26] may occur and destroy useful properties of the material. Our charges 1 and 2 were resistant against SC in the as-quenched state, whereas charge 3 showed some SC on one side and charge 4 on both. Therefore, to study SC susceptibility, we treated charge 1 in detail to produce or to remove SC, with the following results:

Fig. 5a, original, delivery state annealed: no SC

Fig. 5b, cold rolling plus annealing: pronounced SC

Fig. 5c, ground and polished (with 0.25 μm diamond spray polish): pronounced SC; the same after only grinding

Fig. 5d, sharp bending: SC and local shear lines occur

Fig. 5e, local chisel beat: SC from indentation

Fig. 5f, a chemical removal of the disturbed surface layer (about 10 μm removed), done after the mechanical treatments, but before annealing, inhibits the subsequent SC. On the other hand, a relaxation annealing at 300° C for 2 h could not inhibit SC.

These facts should be discussed in the light of some current theoretical considerations. According to [27] surface energy is lowered at certain surfaces such as edges and corners. This means easier nucleation. However, if this was the only reason, the delivery state should also exhibit SC, at least on the dull side of the ribbons.

The stresses induced by the deformation treatments cannot be the reason, because they are removed after the 2 h 300° C annealing. A possible explanation is the enhancement of free energy of the amorphous alloy due to the applied disturbances and local defects. According to Egami [28], two kinds of short range order (SRO) exist in the glassy metal:

(1) topological (structural) SRO, i.e., the atoms occupy certain spaces preferably;

(2) compositional (chemical) SRO, i.e., the different chemical species (atoms) are ordered to each other.

By the local plastic deformations these SROs are disturbed or destroyed, which enhances the free energy and therefore the driving force for crystallization at these locations. It may be mentioned that, during similar experiments [24], SC of the orthorhombic $(FeCo)_3B$ was found after deformations in $Fe_{37.5}Co_{37.5}B_{25}$, but not in $Fe_{40}Co_{40}B_{20}$ nor in $Co_{80}B_{20}$. SC after local bending in FeNiB was interpreted as tearing open of oxide layers or formaton of surface cracks [26]. It seems that, especially in alloys developing several crystal species, the orthorhombic phases $(FeNi)_3B$ or $(FeCo)_3B$ crystallize preferentially from the surface. Since this phase is the thermodynamically stable phase, in contrast to the competing other phases, it may be that due to its higher driving force its growth rate is also the highest.

In summary, all the influences on SC and possible explanations are not yet clear and satisfactory. More work needs to be done in this respect.

Acknowledgement

The authors gratefully acknowledge the supply of specimens from Fa. Vacuumschmelze, Hanau. Thanks are due to Professor Dr H. Warlimont for critical reading of the manuscript.

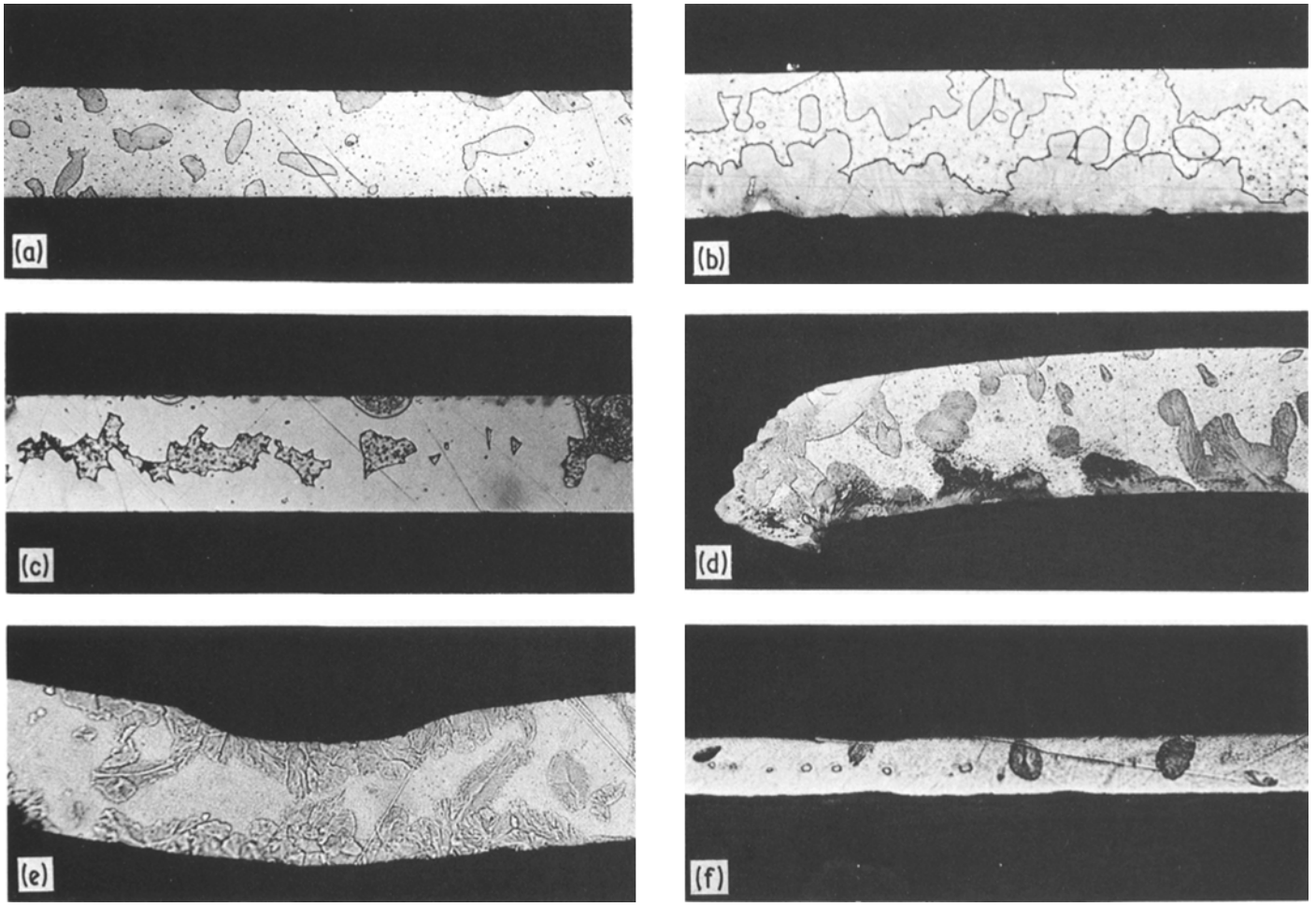

Figure 5 Influence of several treatments on surface crystallization (SC) after 30 min at 385° C. (a) Delivery state annealed, no SC; (b) annealed after cold rolling, SC; (c) ground and polished before annealing, SC; (d) sharp bending before annealing, SC; (e) annealed after a local chisel beat, SC; (f) annealed after a chemical removal of the mechanical disturbed surface layer, no SC.

References

1. J. KÖSTER and U. HEROLD, *J. Phys.* **41** (1980) C-8.
2. M. STUBICAR, *Phys. Stat. Sol. (a)* **44** (1977) 339.
3. A. CZIRAKI, Proceedings of the Conference on Metallic Glasses, Budapest, 1980 (Central Research Institute for Physics, Budapest, 1980).
4. M. von HEIMENDAHL and G. KUGLSTATTER, *J. Mater. Sci.* **16** (1981) 2405.
5. S. RANGANATHAN and M. von HEIMENDAHL, *ibid,* **16** (1981) 2401.
6. R. S. TIWARI, S. RANGANATHAN and M. von HEIMENDAHL, *Z. Metallkd.* **8** (1981) 563.
7. R. S. TIWARI and M. von HEIMENDAHL, *Scripta Met.* **15** (1981) 809.
8. M. von HEIMENDAHL, R. S. TIWARI and J.-C. CLAUS, Proceedings of the 4th Conference on Rapidly Quenched Metals, Sendai, 1981 (Japan Institute of Metals, Sendai, 1982).
9. M. von HEIMENDAHL and G. MAUSSNER, *J. Mater. Sci.* **14** (1979) 1238.
10. M. von HEIMENDAHL, "Electron Microscopy of Materials" (Academic Press, New York, 1980).
11. K. MÜLLER, Diploma Thesis, Universität Erlangen-Nürnberg (1981).
12. J. E. HILLIARD, *Trans. Met. Soc. AIME* **224** (1962) 906.
13. M. von HEIMENDAHL, *Micron* **4** (1973) 111.
14. P. J. GOODHEW and D. CHESCOE, *ibid.* **11** (1980) 153.
15. H. W. STADELMEIER and C. B. POLLOCK, *Z. Metallkd.* **60** (1969) 960.
16. U. HEROLD and U. KÖSTER, *Z. Metallkd.* **69** (1978) 326.
17. J. L. WALTER, S. F. BARTRAM and R. R. RUSSEL, *Met. Trans. A* **9A** (1978) 803.
18. T. WATANABE and M. G. SCOTT, *J. Mater. Sci.* **15** (1980) 1131.
19. J. WONG, F. W. LYTLE, R. B. GREEGOR, H. H. LIEBERMANN, J. L. WALTER and F. E. LUBORSKY, Proceedings of the 3rd Conference on Rapidly Quenched Metals, Brighton 1978 (The Metals Society, London, 1978).
20. U. KÖSTER and U. HEROLD, in "Topics in Applied Physics" Vol. 46, edited by H. J. Güntherodt and H. Beck (Springer, Berlin, Heidelberg, New York, 1981) p. 225.
21. J. A. LEAKE and A. L. GREER, *J. Non-Cryst. Solids* **38 39** (1980) 735.
22. U. HEROLD and U. KÖSTER, Proceedings of the 3rd Conference on Rapidly Quenched Metals, Brighton 1978 (The Metals Society, London, 1978).
23. F. E. LUBORSKY, *Mater. Sci. Eng.* **28** (1977) 139.
24. H. WEISSENBERG, Diploma Thesis, Ruhr-Universität Bochum (1979).
25. F. NOLTE, Diploma Thesis, Ruhr-Universität Bochum (1980).
26. G. TERSTEEGEN, Unpublished work.
27. J. W. CHRISTIAN, "The Theory of Transformations in Metals and Alloys" (Pergamon Press, Oxford, 1975).
28. T. EGAMI, *Mater. Res. Bull.* **13**, (1978) 557.

Received 17 November 1981
and accepted 26 January 1982